Advances in Nano Research, *Vol. 10, No. 3 (2021) 221-234*
DOI: https://doi.org/10.12989/anr.2021.10.3.221

Flow of MHD Powell-Eyring nanofluid: Heat absorption and Cattaneo-Christov heat flux model

Humaira Sharif[1], Mohamed A. Khadimallah[2,3], Muhammad Nawaz Naeem[1], Muzamal Hussain[*1], Sajjad Hussain[4] and Abdelouahed Tounsi[5,6]

[1]*Department of Mathematics, Govt. College University Faisalabad, 38000, Faisalabad, Pakistan*
[2]*Prince Sattam Bin Abdulaziz University, College of Engineering, Civil Engineering Department, Al-Kharj, 16273, Saudi Arabia*
[3]*Laboratory of Systems and Applied Mechanics, Polytechnic School of Tunisia, University of Carthage, Tunis, Tunisia*
[4]*Department of mathematics, Govt Post graduate college, Layyah, Pakistan*
[5]*YFL (Yonsei Frontier Lab), Yonsei University, Seoul, Korea*
[6]*Department of Civil and Environmental Engineering, King Fahd University of Petroleum & Minerals, 31261 Dhahran, Eastern Province, Saudi Arabia*

(*Received July 25, 2020, Revised October 25, 2020, Accepted December 14, 2020*)

Abstract. During the previous few years, phenomenon of bioconvection along with the use of nanoparticles showed large number of applications in technological and industrial field. This paper analyzed the bioconvection phenomenon in magnetohydrodynamic boundary layer flow of a Powell-Eyring nanoliquid past a stretchable cylinder with Cattaneo-Christov heat flux. In addition, the impacts of chemical reaction and heat generation/absorption parameter are considered. By the use of appropriate transformation, the governing PDEs (nonlinear) have been transformed and formulated into nonlinear ODEs. The resulting nonlinear ODEs subjected to relevant boundary conditions are solved analytically through homotopy analysis method which is programmed in Mathematica software. Graphical and numerical results versus physical quantities like velocity, temperature, concentration and motile microorganism are investigated under the impact of physical parameters. It is noted that velocity profile enhances as the curvature parameter A and Eyring-Powell fluid parameter M increases but a decline manner for large values of buoyancy ratio parameter N_r and bio-convection Rayleigh number R_b. In the presence of Prandtl number P_r, Eyring-Powell fluid parameter M and heat absorption parameter δ, temperature profile decreases. Nano particle concentration profile increases for increasing values of magnetic parameter H_a and thermophoresis parameter N_t. The motile density profile has revealed a decrement pattern for higher values of bio-convection Lewis number L_b and bio-convection peclet number P_e. This study may find uses in bio-nano coolant systems, advance nanomechanical bio-convection energy conversion equipment's, etc.

Keywords: Powell-Eyring nanofluid; MHD flow; Cattaneo-Christov heat flux; heat generation/absorption; chemical reaction; bioconvection; HAM

1. Introduction

Nowadays, the nanofluids have been taken into consideration by scientists due to their unique characteristics such as ethylene glycol, propylene glycol and water etc. show less transfer of heat. Nanofluids that are mixture of liquid and solids are commonly used to increase the thermal conductivity of heat transfer in base liquids. Nanofluids shows huge number of applications in industrial fields, microelectronics cooling, towers cooling, best results of hybrid-powered engines and cooling/heating of home electrical appliances, etc (Hsiao 2014, 2016, 2017). Nanofluids are used as a coolant in automobiles and shock absorber to increase the working abilities of air-conditioner and refrigerators. The scientific study of non-Newtonian fluids showed remarkable achievements and its large number of applications in technological fields, biological sciences and in industries. Uses of non-Newtonian fluids in various fields such as cosmetic items, shampoo, polymer solution, power engineering, greases, mixing of food, blood flow and liquid metals flow, etc.

The concept of nanoparticles was given by Choi and Eastman (1995) in order to enhance the heating capacity of base fluids. Many numerical and experimental researches have been carried out by Choi and Eastman (1995) in order to determine how thermal conductivity can be enhanced. Rehman *et al*. (2019) equipped the Williamson fluid in a semi-infinite domain. The ongoing Williamson fluid is interacted with an externally applied magnetic field. The heat transfer individualities are taken into account in the presence of both the heat source and sink. The flow narrating differential system is obtained by coupling the most generally accepted differential equations namely, equation of momentum and equation of energy with constitutive relation of Williamson fluid model. Khan and Pop (2010) presented the boundary layer flow of a nanoliquid through a stretchable surface. They noted that for large values of P_r and reduced Sherwood number.

*Corresponding author, Ph.D. Scholar
E-mail: muzamal45@gmail.com;
muzamalhussain@gcuf.edu.pk

 ISSN: 2287-237X (Print), 2287-2388 (Online)

Prasher *et al*. (2006) discussed the measurements of nanoliquid viscidity and thermal applications. Al-Mdallal *et al*. (2019) investigated the unsteady viscous flow over a shrinking permeable cylinder is investigated in a porous medium under magnetic force. The unsteady Navier-Stokes equations are reduced to ordinary differential equations using a similarity transformation. Numerical technique based on the Iterative Power Series (IPS) method is used to solve the equations for some parameter. Kuznetsov and Nield (2010) analyzed the convective boundary-layer flow of a nanoliquid through a vertical plate. It is investigated that for each *Nr*, *Nt* and *Nb*, dwindle local Nusselt number. Modern advancements related to nanofluids can be found in Subhani and Nadeem (2019), Khan *et al*. (2019), Nadeem *et al*. (2020), Huaxu *et al*. (2020).

Elnajjar *et al*. (2016) presented the unsteady, viscous, and incompressible laminar flow and heat transfer over a shrinking permeable cylinder. The unsteady nonlinear Navier-Stokes and energy equations are reduced, using similarity transformations, to a system of nonlinear ordinary differential equations. In Akbar *et al*. (2015), contrary to the Newtonian fluids, the relationship between strain rate and shear stress is very complicated in non-Newtonian fluids. The well-known flow equation Navier-Stoke's may not amply expressed the remarkable features of non-Newtonian liquids. Thus, to observe the flow rate and phenomenon of transfer of heat for different non-Newtonian liquids, few flow models have been developed depends on their basic features. Model of Eyring Powell fluid within these non-Newtonian liquids which was formulated by Eyring and Powell in 1994. Saranya and Al-Mdallal (2020) studied the basic design of the study is comparison between the magnetohydrodynamic (MHD) flow and heat transfer of non-Newtonian (sodium alginate) base fluid with three ferroparticles, that is cobalt ferrite ($CoFe_2O_4$), manganese-zinc ferrite ($Mn\text{-}ZnFe_2O_4$) and nickel-zinc ferrite ($Ni\text{-}ZnFe_2O_4$) over an unsteady contracting cylinder. Model of Powell-Eyring fluid, having fundamental uses in different industries and geophysical procedures. These essential uses retain forming and fog scattering, designing of different chemical processing instruments, fruit trees groves, temperature distribution and increased oil recovery, etc (Hayat *et al*. 2015). Eyring Powell fluid has extra-ordinary characteristics. Therefore, at the present age there are scientists who are researching on Eyring-Powell liquid models. Besthapu *et al*. (2019) examined the present analysis the combine effects of thermal radiation and velocity slip along a convectively nonlinear stretching surface. Moreover, MHD effects are also considered near the stagnation point flow of Casson nanofluid. Slipped effects are considered with the porous medium to reduce the drag reduction at the surface of the sheet. Main structure of the system is based upon the system of partial differential equations attained in the form of momentum, energy and concentration equations.

Such as Malik *et al*. (2013) reported the boundary layer flow of Eyring Powell nanoliquid model past a stretchable cylinder dependent on temperature possess variable viscidity. Further, modern attempts on Eyring-Powell nanofluid can be seen through Riaz *et al*. (2019), Umar *et al*. (2019), Zubair *et al*. (2019), Alwatban *et al*. (2019). Soomro *et al*. (2018) adjusted the heat generation/ absorption effects in the presence of nonlinear thermal radiation along a moving slip surface. Uniform magnetic field and convective condition along the stretching surface are adjusted to deal the slip mechanisms in term of Brownian motion and thermophoresis for nanofluid. The mathematical model described by Fourier for transfer of heat in materials is represented as $q = -k\nabla T$, where denotes heat flux vector, T is temperature. Physical analysis of Fourier heat transfer is the basic interruption expeditiously experienced by surface which is the main restriction of it. In year 1948, Cattaneo (1948) control this problem and he includes thermal relaxation to Fourier's rule. Ragupathi *et al*. (2019) showed the numerical analysis on the steady, three dimensional flows of different nanofluids past a Riga plate with non-uniform heat source/sink effects. Similarity transformations were used for the conversion of the partial differential equations that govern the flow to the ordinary differential equations. Mishra *et al*. (2018) studied the free convective micropolar fluid over a shrinking sheet in presence of heat source/sink. The method of solution involves similarity trans-formation. The coupled non-linear partial differential equations representing momentum and concentration and non-homogeneous heat equation are reduced into set of non-linear ordinary differential equations. Christov (2009) make improvement the Cattaneo's model. This model is familiar as Cattaneo-Christov heat flux. Straughan (2008, 2020) investigated the process of transfer of heat with thermal convection by the use of Cattaneo heat flux. Cattaneo-Christov heat flux by use of Maxwell nanofluid with slip impact was explored by Han *et al*. (2014). The exponential stretchable flow of viscoelastic liquid by utlizing Cattaneo-Christov model was numerically investigated by Khan *et al*. (2015). Chaudhary and Merkin (1995) examined the reaction of homogeneous-heterogeneous and isothermal model.

The magneto-hydrodynamics is the branch of science which discusses the important interactions of the magnetic field and the movement of electrical conducting liquids such as hot ionizes gases, fluid metals and strong electrolytes. Magneto-hydrodynamics flow shows large number of applications in engineering and field of technology for example electric motors, in design of cooling systems, measurement of blood flow, magneto-hydrodynamics generators, flow meters and pumps, etc (Hayat *et al*. 2014). However, many scientists find out the properties of magneto-hydrodynamics flow. The study of MHD stream line flow in free convection of passing nanoliquids through a vertical permeable surface under acceleration is observed by Freidoonimehr *et al*. (2015). They reported that by minimizing the coefficient of skin fraction, nano-particles volume fraction and magnetic parameter enhance. Stagnation point flow of a hybrid nanoliquid passing through a stretchable surface under the impact of an induced magnetic field was investigated by Ghadikolaei *et al*. (2017). They found that by enhancing the magnetic parameter, coefficient of skin friction decline and reciprocal magnetized Prandtl number enhances. Magneto-

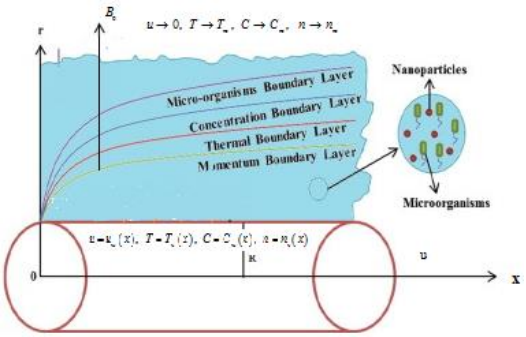

Fig. 1 Flow geometry of the physical model

hydrodynamics fluid flow and transfer of heat through a two-three dimensional permeable and deformation surface was discussed by Mustafa (2016). Shah *et al*. (2019) explored the impact of non-linear thermal radiation on magneto-hydrodynamics nanoliquid thin film flow through a horizontal rotatable disk. Their result shows that for higher values of magnetic coefficient, thin film thickness of nanoliquids decay. Zhao *et al*. (2019) discussed the heat transfer of the magneto-hydrodynamics nanoliquid through permeable micro-tubes in the presence of electro-kinetic impacts. Some latest and impressive articles can be found in Ma *et al*. (2019), Zangooee *et al*. (2019), Ahmed *et al*. (2019), Alkanhal *et al*. (2019), Abbas *et al*. (2020), Tlili *et al*. (2020).

The scientific studies on bio-convective nanoliquid flow over a stretchable surface are now an interesting topic for the scientists in current time period because of its large number of utilizations in industries. Bio-convective process is used in many micro-systems for example biotechnology due to their mixing property to increase the mass transport. The microbial increased oil recovery procedure is used to enhance oil recovery in gas and oil industries (Begum *et al*. 2017). It is widely used in biomedicine fields (delivery of nanodrug and cancer therapy), biotechnology, etc. it is familiar that bio-convection process happened because of density gradient of the gyrotactic microorganisms. These gyrotactic micro-organisms show self-movement and can swim vigorously in water. Few stimuli for example oxygen gradient, chemical substances and gravity help these motile microorganisms move in an upper direction. Micro-organisms are mixed with the less concentrate suspension of nanoparticles to enhance stability of nanoliquid and to control nanoparticle agglomeration in nanoliquids (Abdul Latiff *et al*. 2016, Ahmed and Mahdy *et al*. 2016, Khan *et al*. 2020). Recently some researcher used different methods for nonlinear modeling (Eltaher *et al*. 2019, Ebrahimi *et al*. 2019, Safaei *et al*. 2019, Shahsavari *et al*. 2019, Benmansour *et al*. 2019).

The homotopy analysis method is very successful semi-analytic approximation method to solve the highly non-linear equations in engineering, science and finance. The term homotopy was introduced from topology in order to generate convergence series solution for nonlinear system. Homotopy analysis method is such a series which directly does not depend upon large or small parameters. This method is useful for nonlinear system. Many authors (Doh *et al*. 2020, Mittal 2019, Reddy *et al*. 2018) employed the homotopy analysis method to solve the boundary layer problems.

The above-discussed literature reveals that no research work exists on bio-convection nanofluid flow, considering the impact of heat absorption/generation and chemical reaction parameter containing motile microorganisms over a stretching cylinder. As far as we know, for such type of problems, there does not exist any solution by using HAM. Hence, the novelty of this article is to observe the boundary layer flow of a Powell-Eyring nanoliquid over a horizontal stretchable cylinder with bioconvection of nanoliquid comprising motile microorganisms. The effect of heat sink/source and chemical reaction are also analyzed.

2. Formulation of the problem

We consider an axisymmetric and magnetohydro-dynamic laminar steady boundary layer flow of a Powell-Eyring nanoliquid past a stretched cylinder of R radius in the presence of motile microorganism. Further, the energy equation is extended by adding heat generation and absorption parameter. The chemical reaction coefficient is utilized in concentration equation. Since cylinder is stretchable so flow of Eyring-Powell nanoliquid is along x direction. R is the radial coordinate take perpendicular to cylinder axis. In cylindrical coordinates, x-axis is with axis of the cylinder and we considered r-axis is with radial direction it is presented in Fig. 1. n_∞, C_∞ and T_∞ represents the free stream microorganism, concentration and temperature. Under these suppositions, the governing equations are constituted as Kuznetsov (2010), Ibrahim and Hindebu (2019), Aziz *et al*. (2018).

$$\frac{\partial(ru)}{\partial x}+\frac{\partial(rv)}{\partial r}=0 \tag{1}$$

$$\begin{aligned}&\frac{\partial u}{\partial x}+v\frac{\partial u}{\partial r}=\frac{\mu}{\rho}\left(\frac{\partial^2 u}{\partial r^2}+\frac{1}{r}\frac{\partial u}{\partial r}\right)+\frac{1}{\rho\beta c}\left(\frac{\partial^2 u}{\partial r^2}+\frac{1}{r}\frac{\partial u}{\partial r}\right)\\&-\frac{1}{6\rho\beta c^3}\left[\frac{1}{r}\left(\frac{\partial u}{\partial r}\right)^3+3\left(\frac{\partial u}{\partial r}\right)^2\frac{\partial^2 u}{\partial r^2}\right]-\frac{\sigma' {B_0}^2}{\rho}u\\&+\frac{1}{\rho}\begin{bmatrix}(1-C_\infty)\rho\beta g(T-T_\infty)\\-(\rho_p-\rho)g(C-C_\infty)-(n-n_\infty)g\gamma(\rho_m-\rho)\end{bmatrix}\end{aligned} \tag{2}$$

$$\begin{aligned}&\lambda_E'\begin{bmatrix}u^2\frac{\partial^2 T}{\partial x^2}+v^2\frac{\partial^2 T}{\partial r^2}+2uv\frac{\partial^2 T}{\partial x\partial r}+u\frac{\partial T}{\partial x}\frac{\partial u}{\partial x}\\+u\frac{\partial T}{\partial r}\frac{\partial v}{\partial x}+v\frac{\partial T}{\partial x}\frac{\partial u}{\partial r}+v\frac{\partial T}{\partial r}\frac{\partial v}{\partial r}\end{bmatrix}\\&+u\frac{\partial T}{\partial x}+v\frac{\partial T}{\partial r}=\alpha_f'\left(\frac{\partial^2 T}{\partial r^2}+\frac{1}{r}\frac{\partial T}{\partial r}\right)\\&+\tau\left(D_B\frac{\partial T}{\partial r}\frac{\partial C}{\partial r}+\frac{D_T}{T_\infty}\left(\frac{\partial T}{\partial r}\right)^2\right)+Q_0'\frac{(T-T_\infty)}{(\rho c)_f}\end{aligned} \tag{3}$$

$$\lambda_c'\begin{bmatrix}u^2\frac{\partial^2 C}{\partial x^2}+v^2\frac{\partial^2 C}{\partial r^2}+2uv\frac{\partial^2 C}{\partial x\partial r}+u\frac{\partial C}{\partial x}\frac{\partial u}{\partial x}\\+u\frac{\partial C}{\partial r}\frac{\partial v}{\partial x}+v\frac{\partial C}{\partial x}\frac{\partial u}{\partial r}+v\frac{\partial C}{\partial r}\frac{\partial v}{\partial r}\end{bmatrix} \tag{4}$$

$$+u\frac{\partial C}{\partial x}+v\frac{\partial C}{\partial r}=D_B\left(\frac{\partial^2 C}{\partial r^2}+\frac{1}{r}\frac{\partial C}{\partial r}\right)+\frac{D_T}{T_\infty}\left(\frac{\partial^2 T}{\partial r^2}+\frac{1}{r}\frac{\partial T}{\partial r}\right)-R_r(C-C_\infty) \quad (4)$$

$$u\frac{\partial n}{\partial x}+v\frac{\partial n}{\partial r}+\frac{bW_c}{(C_w-C_\infty)}\left[\frac{\partial}{\partial r}\left(n\frac{\partial C}{\partial r}\right)\right]=D_m\left(\frac{\partial^2 n}{\partial r^2}\right) \quad (5)$$

The boundary conditions are

$$\begin{aligned} &u=u_w=u_0\left(\frac{x}{l}\right), \qquad v(x,r)=0\\ &T(x,r)=T_w=T_\infty+T_0\left(\frac{x}{l}\right)\\ &C(x,r)=C_w=C_\infty+C_0\left(\frac{x}{l}\right)\\ &n(x,r)=n_w \quad \text{at} \quad r=R \end{aligned} \quad (6)$$

$$\begin{aligned} &u\to u_\infty, \qquad T\to T_\infty, \qquad C\to C_\infty\\ &n\to n_\infty \qquad \text{at} \qquad r\to\infty \end{aligned} \quad (7)$$

where *u* and *v* denote the velocity components along *x*- and *r*-directions, respectively.

Presenting the suitable conversions

$$\begin{aligned} &\eta=\frac{r^2-R^2}{2R}\sqrt{\frac{u_0}{\nu l}}, \qquad \psi=\sqrt{u_w\nu x}Rf(\eta)\\ &u=u_w f'(\eta), \qquad v=-\frac{R}{r}\sqrt{\frac{\nu u_0}{l}}f(\eta)\\ &\theta(\eta)=\frac{T-T_\infty}{T_w-T_\infty}, \quad \phi(\eta)=\frac{C-C_\infty}{C_w-C_\infty}, \quad \chi(\eta)=\frac{n-n_\infty}{n_w-n_\infty} \end{aligned} \quad (8)$$

where η is similarity variable, ψ is stream function, $f(\eta)$ is dimensionless stream function, θ, ϕ and χ are dimensionless temperature, concentration and microorganism distributions respectively.

After applying Eq. (8), equation of continuity Eq. (1) is satisfied while the governing equations Eq. (2) to Eq. (5) are converted into non-linear ODE's.

$$\begin{aligned} &(1+M)(1+2A\eta)f'''+ff''-f'^2+2A(1+M)f''\\ &-\frac{4}{3}M\lambda A(1+2A\eta)f''^3-M\lambda(1+2A\eta)^2f'''f''^2\\ &-{H_a}^2f'+\Omega(\theta-Nr\phi-Rb\chi)=0 \end{aligned} \quad (9)$$

$$\begin{aligned} &\frac{(1+2A\eta)}{Pr}\theta''+\frac{2A}{Pr}\theta'+f\theta'-\beta_t(f^2\theta''+ff'\theta')\\ &+Nb(1+2A\eta)\theta'\phi'+Nt(1+2A\eta)\theta'^2+\delta\theta=0 \end{aligned} \quad (10)$$

$$\begin{aligned} &(1+2A\eta)\phi''+2A\phi'+Lef\phi'-Le\beta_c(f^2\phi''+ff'\phi')\\ &+\frac{Nt}{Nb}(1+2A\eta)\theta''+2A\frac{Nt}{Nb}\theta'-Le\tau\phi=0 \end{aligned} \quad (11)$$

$$\begin{aligned} &(1+2A\eta)\chi''+Lbf\chi'-Pe(1+2A\eta)\\ &(\phi''(\chi+\Omega_1)+\phi'\chi') \end{aligned} \quad (12)$$

The equivalent boundary conditions are

$$\begin{aligned} &f(0)=0, \qquad f'(0)=1, \qquad \theta(0)=1\\ &\phi(0)=1, \qquad \chi(0)=1 \end{aligned} \quad (13)$$

$$\begin{aligned} &f'(\infty)=0, \qquad \theta(\infty)=0, \qquad \phi(\infty)=0,\\ &\chi(\infty)=0 \end{aligned} \quad (14)$$

where $M=\frac{1}{\mu\beta c}$, $\lambda=\frac{a^3x^2}{2c^2\nu}$, $a=\frac{u_0}{l}$ are Eyring-Powell fluid parameters, $Ha=\frac{\sigma{B_0}^2l}{\rho u_0}$ is magnetic parameter, $A=\frac{1}{R}\sqrt{\frac{\nu}{a}}$ is curvature parameter, $\Omega=\frac{\beta(1-C_\infty)(T_w-T_\infty)}{{u_0}^2}$ is mixed convection, $Nr=\frac{(\rho_p-\rho)(C_w-C_\infty)}{(1-C_\infty){u_0}^2(T_w-T_\infty)\beta}$ is buoyancy ratio, $Rb=\frac{\gamma(\rho_m-\rho)(n_w-n_\infty)}{(1-C_\infty){u_0}^2(T_w-T_\infty)}$ is bioconvection Rayleigh number, $Pr=\frac{\nu}{\alpha}$ is Prandtl number, $\beta_t=\frac{\lambda_E' u_0}{l}$ is thermal relaxation parameter, $Nb=\frac{\tau D_B(C_w-C_\infty)}{\nu}$ is Brownian motion parameter, $Nt=\frac{\tau D_T(T_w-T_\infty)}{T_\infty\nu}$ is thermophoresis parameter, $\delta=\frac{Q_o' l}{(\rho c)_f u_0}$ is heat absorption/generation parameter, $Le=\frac{\nu}{B_B}$ is Lewis number $\beta_c=\frac{\lambda_c' u_0}{l}$ is concentration relaxation parameter, $\tau=\frac{R_r l}{u_0}$ is chemical reaction coefficient, $Pe=\frac{bW_c}{D_m}$ denotes the Peclet number, $Lb=\frac{\nu}{D_m}$ is bio-convection Lewis number, $\Omega_1=\frac{n_\infty}{n_w-n_\infty}$ is concentration difference parameter.

2.1 Some physical quantities

Here skin friction coefficient C_f is

$$C_f=\frac{2\tau_w}{\rho{u_w}^2} \quad (15)$$

The wall shear stress at $r = R$ becomes

$$\tau_w=[S]_{r=R}=\left[\mu\left(\frac{\partial u}{\partial r}\right)+\frac{1}{\beta c}\left(\frac{\partial u}{\partial r}\right)-\frac{1}{6\beta c^3}\left(\frac{\partial u}{\partial r}\right)^3\right]_{r=R} \quad (16)$$

Hence, by Eq. (15) and Eq. (16) the non-dimensional form of coefficient of skin friction is

$$\frac{1}{2}C_f\sqrt{Re_x}=(1+K)f''(0)-\frac{K}{3}\lambda f''^3(0) \quad (17)$$

The related formulas for local Nusselt number Nu_x, local Sherwood number Sh_x and motile density number Nn_x as follows

$$\begin{aligned} &Nu_x=\frac{xq_1}{k(T_w-T_\infty)}, \qquad Sh_x=\frac{xj_1}{D_B(C_w-C_\infty)}\\ &Nn_x=\frac{xg_1}{D_B(n_w-n_\infty)} \end{aligned} \quad (18)$$

Here $q_1=-k\left(\frac{\partial T}{\partial r}\right)_{r=R}$ is surface heat flux, $j_1=-D_B\left(\frac{\partial C}{\partial r}\right)_{r=R}$ is surface mass flux, $g_1=-D_m\left(\frac{\partial n}{\partial r}\right)_{r=R}$ is motile microorganism flux. After the use of Eq. (18), we obtained the following transformed form.

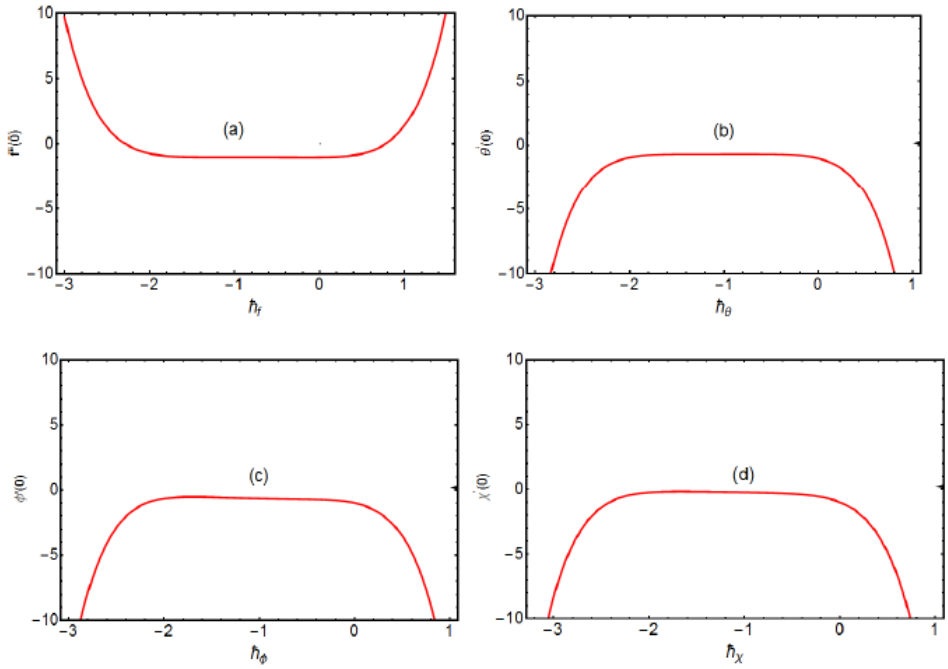

Fig. 2 Convergent $\hbar$-curves for non-linear ODE's

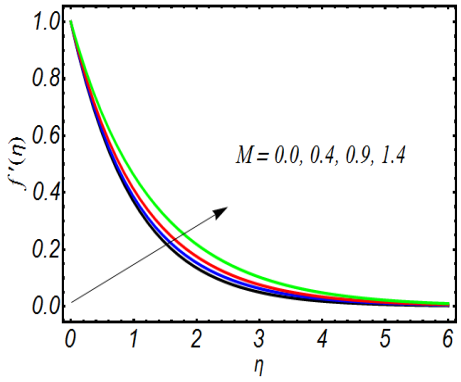

Fig. 3 Characteristics of f' via M

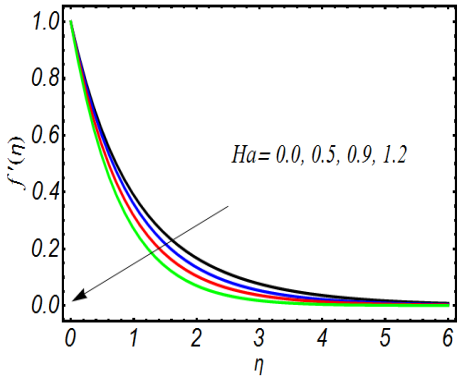

Fig. 4 Characteristics of f' via Ha

$$\frac{Nu_x}{\sqrt{Re_x}} = -\theta'(0), \qquad \frac{Sh_x}{\sqrt{Re_x}} = -\phi'(0) \qquad \frac{Nn_x}{\sqrt{Re_x}} = -\chi'(0) \tag{19}$$

2.2 Homotopy analysis method

According to this fluid model that is governed by the highly nonlinear equations for which exact solution cannot be obtained. So, we assumed the alternate method to calculate the series solution by the use of homotopy analysis approach. Introduced by Liao (2014), many authors used this approach to obtain the series solution based on many mathematical models Shehzad (2018), Turkyilmazoglu (2016a). We considered suitable initial guesses as given below

$$f_0(\eta) = 1 - e^{-\eta}, \qquad \theta_0(\eta) = e^{-\eta}, \qquad \phi_0(\eta) = e^{-\eta} \qquad \chi_0(\eta) = e^{-\eta} \tag{20}$$

The linear operators (L_f, L_θ, L_ϕ, L_χ) are chosen as follow

$$L_f = f''' - f', \qquad L_\theta = \theta'' - \theta, \qquad L_\phi = \phi'' - \phi \qquad L_\chi = \chi'' - \chi \tag{21}$$

Satisfying

$$L_f[A_1 + A_2 e^{\eta} + A_3 e^{-\eta}] = 0, \quad L_\theta[A_4 e^{\eta} + A_5 e^{-\eta}] = 0, \quad L_\phi[A_6 e^{\eta} + A_7 e^{-\eta}] = 0 \quad L_\chi[A_8 e^{\eta} + A_9 e^{-\eta}] = 0 \tag{22}$$

in which A_i (i = 1, 2, 3, ….9) are the arbitrary constants.

3. Convergence analysis

The homotopic approach gives us a wonderful flexibility to select the auxiliary parameters $\hbar_f$, $\hbar_\theta$, $\hbar_\phi$ and $\hbar_\chi$ regarding series solutions adjustment and control the convergence. So, relevant $\hbar$-curves are shown in Fig. 2.

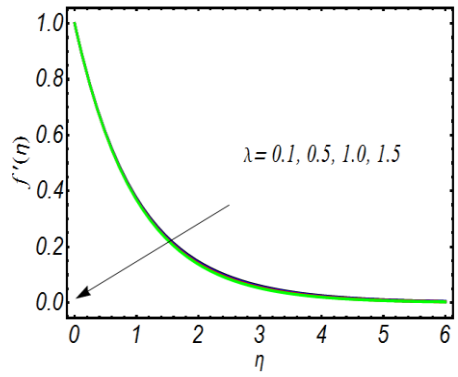

Fig. 5 Characteristics of f' via λ

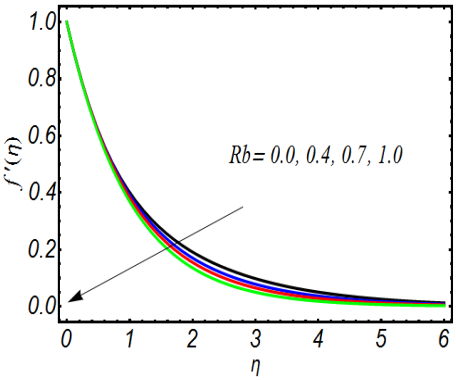

Fig. 8 Characteristics of f' via Rb

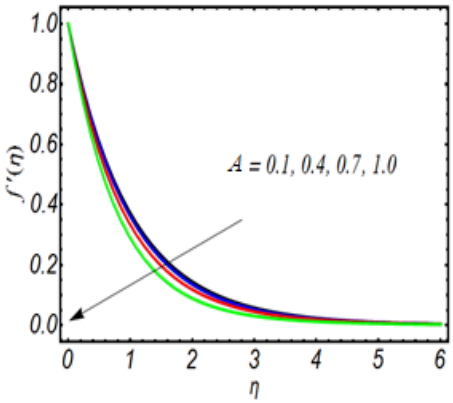

Fig. 6 Characteristics of f' via A

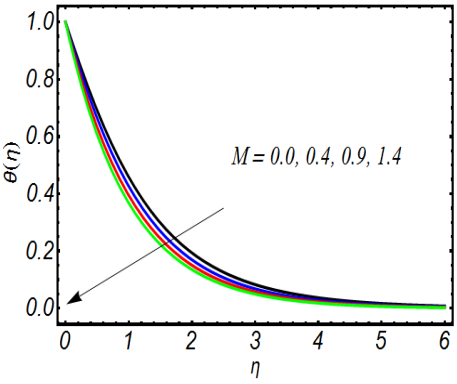

Fig. 9 Characteristics of θ via M

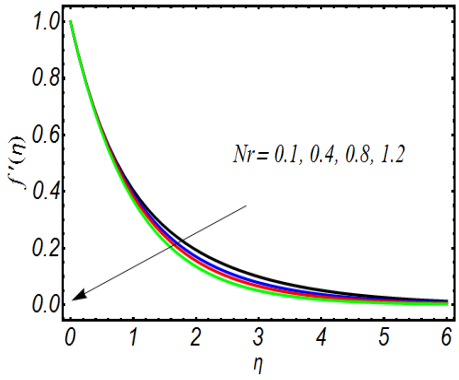

Fig. 7 Characteristics of f' via Nr

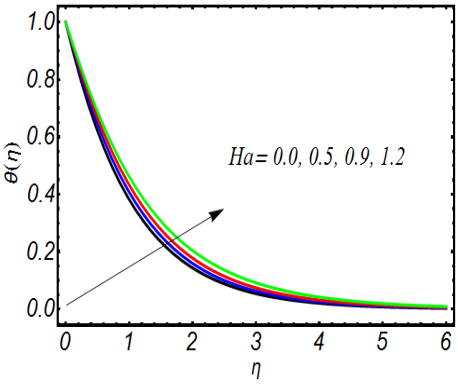

Fig. 10 Characteristics of θ via Ha

The suitable convergence values of such problem are $-2.0 \leq \hbar_f \leq 0.8$, $-2.0 \leq \hbar_\theta \leq 0.1$, $-2.0 \leq \hbar_\phi \leq 0.1$, $-2.0 \leq \hbar_\chi \leq -0.1$.

4. Discussion section

In this portion, the impact of various parameters i.e. Powell-Eyring fluid parameters M and λ, magnetic field parameter Ha, curvature parameter A, mixed convection constant σ', buoyancy ratio parameter Nr, bio-convected Rayleigh number Rb, Prandtl number Pr, Brownian motion Nb, thermophoresis parameter Nt, heat source/sink coefficient δ, thermal relaxation parameter β_t, Lewis number Le, chemical reaction τ, concentration relaxation parameter β_c, bio-convection Peclet number Pe, bio-convection Lewis number Lb through graphically and tabular form.

Fig. 3 is sketched to elucidate the effect of Powell-Eyring fluid parameter M on velocity distribution. It is notice that velocity profile intensifies with the increasing values of M. Because the fluid parameter M has reverse relationship with viscidity, so the large values of M represents the liquid to be less viscid and hence enhancement in deformation rate. The effect of magnetic parameter Ha over velocity distribution is sketched in Fig. 4. It is noticed that for large values of Ha the velocity

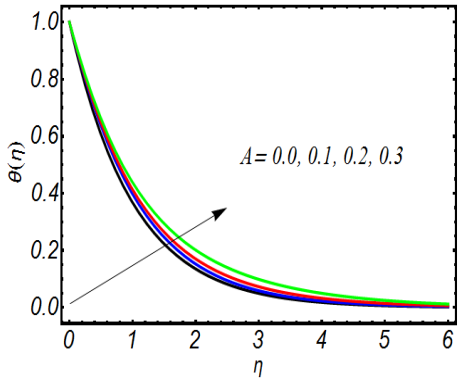

Fig. 11 Characteristics of θ via A

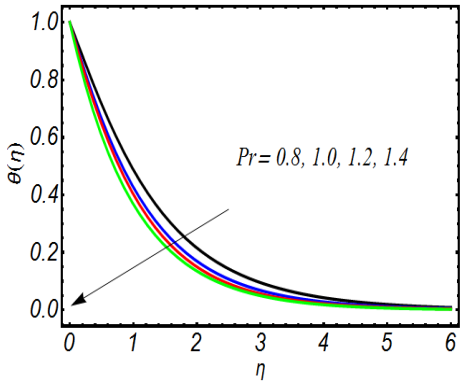

Fig. 12 Characteristics of θ via Pr

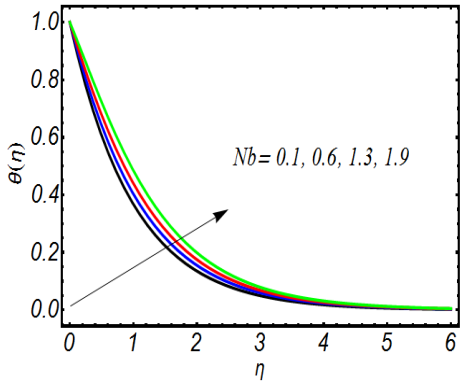

Fig. 13 Characteristics of θ via Nb

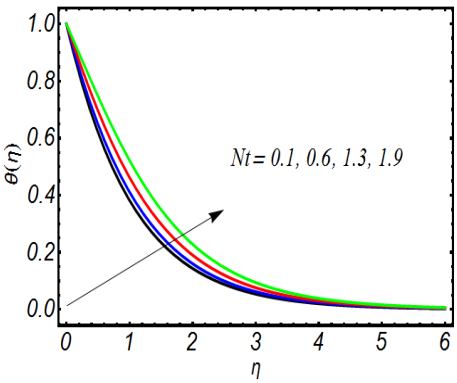

Fig. 14 Characteristics of θ via Nt

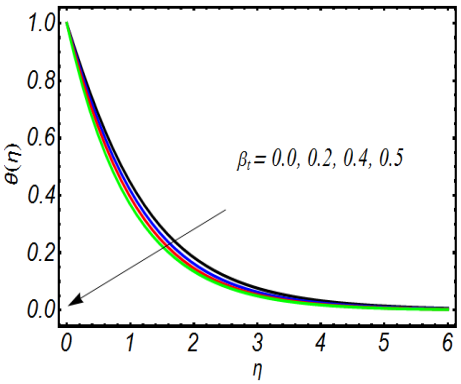

Fig. 15 Characteristics of θ via β_t

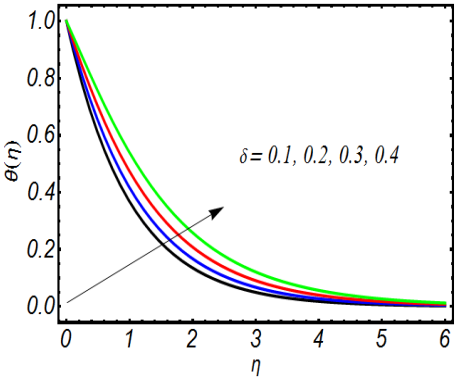

Fig. 16 Characteristics of θ via δ

profile decreases. Physically, for large magnetic parameter *Ha* the resistive force which is well-known as Lorentz force becomes significant to cause the velocity distribution diminishes. Fig. 5 indicates the effect of fluid parameter λ on velocity field. It is clear from the figure that the velocity field decreases for large values of fluid parameter λ. Fig. 6 is given the Influence of mixed convection constant σ' over velocity distribution. It is observed that for large values of mixed convection constant σ', the velocity distribution retarded. This is because, mixed convection constant σ' shows link with buoyancy force that retain resistive property. Figs. 7 and 8 are prepared to observe the behavior of buoyancy ratio parameter *Nr* and bio-convected Rayleigh number *Rb* on the velocity distribution. Clearly velocity distribution is a decreasing function of *Nr* and *Rb*. The reason behind this both *Nr* and *Rb* are liable for the interaction of buoyancy forces which defy the movement of fluid particles in the whole domain.

Fig. 9 describes the impact of Powell-Eyring fluid parameter *M* on temperature distribution. It is noticed that as value of *M* rises the thickness of thermal boundary layer and temperature distribution are retarded gradually. The reason beyond this for large values of *M* liquid becomes lesser viscous therefore friction between liquid layer diminish consequently temperature decreases. Thus, temperature for viscid liquid is larger than that of Powell-Eyring nanofluid in stretchable cylinder. Fig. 10 visualizes the effect of *Ha* on temperature distribution. It is noticed

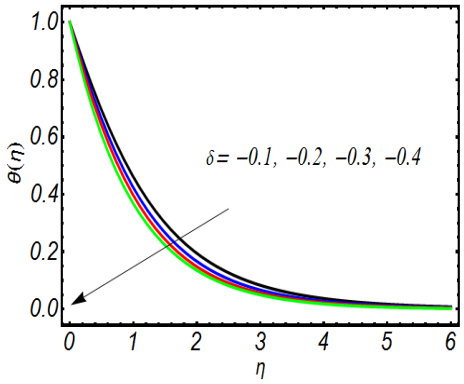

Fig. 17 Characteristics of θ via δ

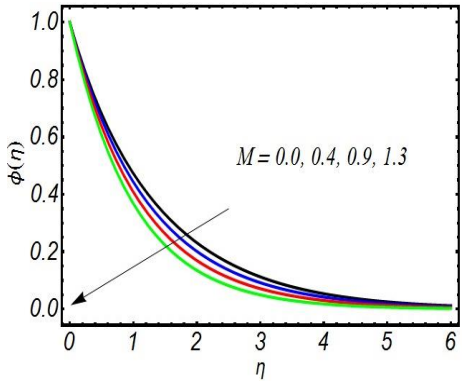

Fig. 18 Characteristics of ϕ via M

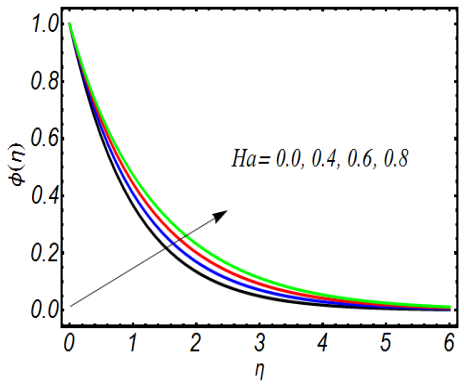

Fig. 19 Characteristics of ϕ via Ha

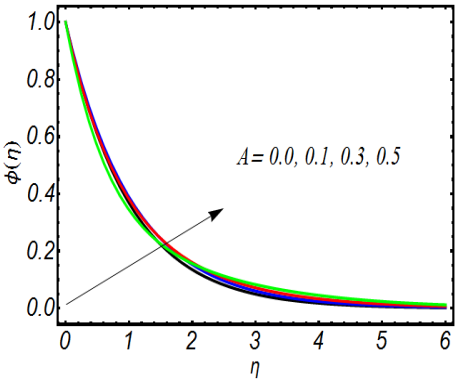

Fig. 20 Characteristics of ϕ via A

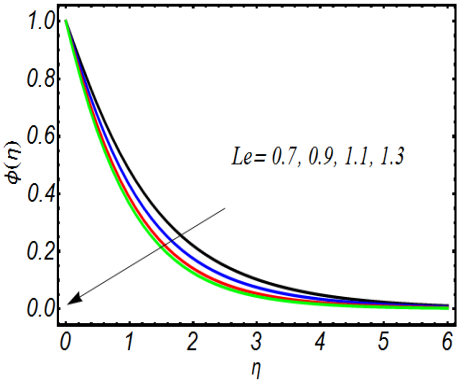

Fig. 21 Characteristics of ϕ via Le

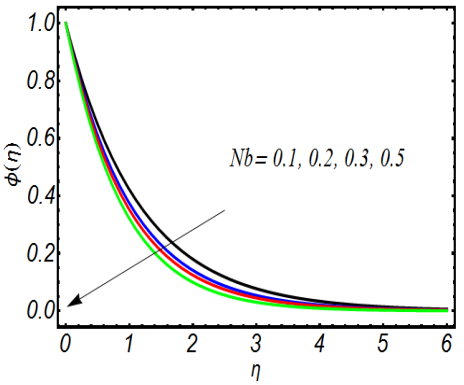

Fig. 22 Characteristics of ϕ via Nb

that for large values of Ha, thermal boundary layer distribution increases. Physically, magnetic parameter involves Lorentzian force which intensify the temperature field. Fig. 11 portrays the impact of curvature parameter Aon temperature field. For large values of A, increases the temperature field. Physically thickness of thermal boundary layer enhance as the curvature parameter A enhance due to which rate of heat transport decline and hence fluid temperature enhances. Fig. 12 shows the influence of Pr on temperature profile. Temperature profile decreases for large values of Prandtl number Pr. It is well-known fact that thermal diffusivity and Prandtl number Pr have reverse relationship due to which for large values of Pr result in temperature reduces. Fig. 13 illustrates the influence of Brownian motion parameter Nb on temperature field. It is noted that increment in Brownian motion Nb, temperature distribution increases. Physically an increment in Nb, random movement of liquid particles intensify so temperature distribution rises. Fig. 14 demonstrates the influence of thermophoresis parameter Nt on temperature field. For enhancing values of Nt, temperature field is increases. The reason is that an increment in Nt produce a robust thermophoretic force which allow migration of small particles warm to cold surface due to which temperature field enhance. Effect of thermal relaxation parameter β_t on temperature profile is sketched in Fig. 15. It is noted that large values of β_t shows a declining behavior for temperature distribution. The reason is that for transfer of

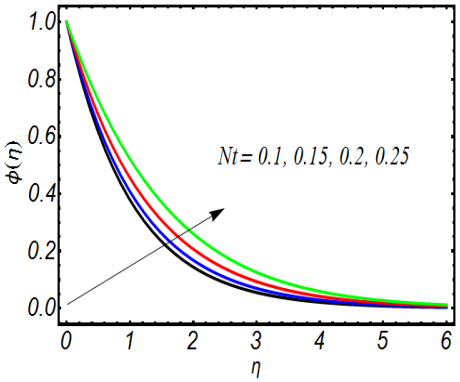

Fig. 23 Characteristics of ϕ via Nt

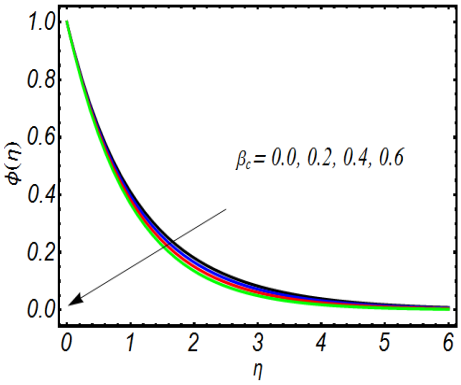

Fig. 24 Characteristics of ϕ via β_t

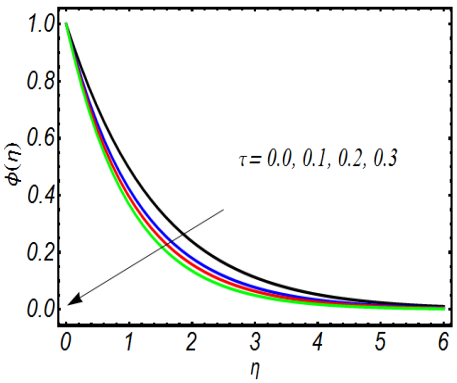

Fig. 25 Characteristics of ϕ via τ

heat energy between fluid particles and its surrounding needs time relaxation. Hence, with the increase in value of β_t the particles of material require more time for transfer of heat to its neighboring particles as a result decrement in temperature is observed. However, by enhancing the value of time relaxation parameter β_t less heat transfer from medium of the cylinder to the liquid is observed. In Figs. 16 and 17, the heat generation/absorption parameter δ is shown graphically. It is observed that for large values of heat absorption parameter $\delta < 0$ reduces the temperature of Eyring-Powell nanofluid although it increases for the heat generation $\delta > 0$. As the heat generation occurrence added some additional heat to the fluid which raises the temperature distribution.

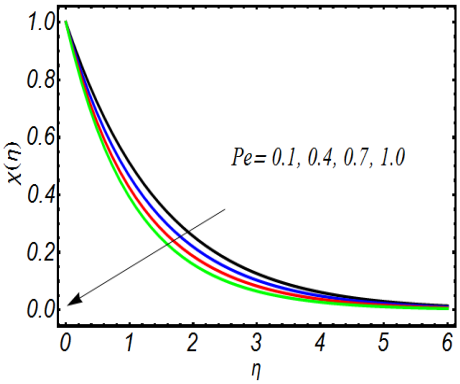

Fig. 26 Characteristics of χ via Pe

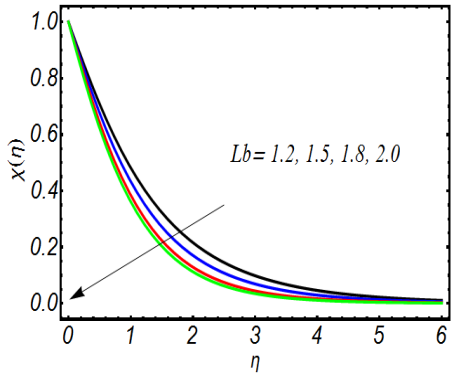

Fig. 27 Characteristics of χ via Lb

Table 1 Numerical data of $f''(0)$ for dissimilar values of $M = \lambda = Le = Nt = Nb = Nr = Nc = Lb = Ha = 1/10$, $Pr = Pe = 1$, $\beta_t = \beta_c = 1/10$

M	λ	Ha	A	Nr	Nc	$-f''(0)$
0.1	0.1	0.1	0.1	0.1	0.1	1.1415
0.2						1.1884
0.3						1.2355
	0.1					1.1415
	0.5					1.1351
	0.9					1.1321
		0.1				1.1415
		0.2				1.1567
		0.3				1.1818
			0.1			1.1415
			0.2			1.1846
			0.3			1.2266
						1.1415
						1.2335
						1.3327
				0.1		1.1415
				0.2		1.1356
				0.3		1.1304
					0.1	1.1415
					0.2	1.1351
					0.3	1.1306

Influence of Powell-Eyring fluid parameter M on

Table 2 Numerical data of $f''(0)$ for dissimilar values of $M = \lambda = Le = Nt = Nb = Nr = Nc = Lb = Ha = 1/10$, $Pr = Pe = 1$, $\beta_t = \beta_c = 1/10$

M	λ	Ha	A	Pr	Nb	Nt	Le	β_t	$-\theta'(0)$
0.1	0.1	0.1	0.2	1.0	0.1	0.1	0.1	0.1	0.6836
0.3									0.6956
0.5									0.7053
	0.1								0.6836
	0.5								0.6829
	0.9								0.6821
		0.1							0.6836
		0.2							0.6813
		0.6							0.6776
			0.2						0.6836
			0.5						0.7603
			0.7						0.8163
				1.0					0.6836
				1.2					0.7485
				1.4					0.8052
					0.1				0.6836
					0.2				0.6252
					0.3				0.5732
						0.1			0.6836
						0.2			0.6755
						0.3			0.6624
							0.1		0.6836
							0.3		0.6792
							0.5		0.6750
								0.1	0.6836
								0.3	0.6939
								0.6	0.7093

Table 3 Numerical data of $\phi'(0)$ for dissimilar values of $Nr = Nc = Lb = \tau = 1/10$, $Pr = Pe = 1$, $\beta_t = \beta_c = 1/10$

M	λ	Ha	A	Nb	Nt	Le	βc	$-\phi'(0)$
0.4	0.1	0.2	0.1	0.1	0.1	1.3	0.1	0.9846
0.6								0.9848
0.7								0.9851
	0.1							0.9846
	0.5							0.9845
	0.6							0.9844
		0.2						0.9846
		0.4						0.9844
		0.6						0.9841
			0.1					0.9846
			0.11					0.9890
			0.22					1.0544
				0.1				0.9846
				0.15				1.0690
				0.2				1.1354
					0.1			0.9846
					0.2			0.6726
					0.3			0.5387
						1.3		0.9846
						1.5		1.0084
						1.7		1.0188
							0.1	0.9846
							0.3	0.9757
							0.5	0.9646

Table 4 Numerical data of $\chi'(0)$ for dissimilar values of $\lambda = Le = Nt = Nb = Ha = 1/10$, $Pr = 1$, $\beta_t = \beta_c = 1/10$

M	Nr	Rb	Lb	Pe	$-\chi'(0)$
0.1	0.2	0.2	2.0	0.1	0.9842
0.2					0.9844
0.3					0.9845
	0.2				0.9842
	0.3				0.9821
	0.5				0.9799
		0.2			0.9842
		0.3			0.9792
		0.5			0.9654
			1.2		0.9791
			1.5		0.9798
			1.8		0.9820
				0.1	0.9842
				0.2	0.9799
				0.5	0.9791

concentration field is revealed in Fig. 18. It is investigated that both concentration distribution and thickness of concentration boundary layer decline with an increment in M. Fig. 19 illustrates the impact of magnetic parameter Ha on concentration profile. It has been examined that enhancing the values of Ha, both concentration distribution and thickness of concentration boundary layer improves. Fig. 20 represents the curvature parameter on the concentration profile. The value of concentration profile decreases on increasing the similarity variable η. The effect of different curvature parameter is seen in this graph.

Fig. 21 portrays the impact of Lewis number Le on concentration distribution. The drawn result shows that when we assign largest values to Lewis number, concentration distribution decreases. Physically Lewis number has direct relationship with mass diffusion which reduces the concentration profile. Fig. 22 demonstrates that how Brownian motion parameter Nb affects the concentration distribution. When we assign the maximum values to Nb, concentration distribution and thickness of concentration boundary layer reduces. Physically as Nb increases, the random movement and collision of small particles of the liquid enhance which decline the fluid concentration. The behavior of thermophoresis parameter Nt on concentration field is displayed in Fig. 23. It is investigated that as the values of Nt enhance, thickness of concentration boundary layer and concentration field boosted. Physically, with higher values of Nt many nano-particles are pushed away from warm surface, due to this concentration of nano-particles increases. Influence of concentration relaxation parameter β_c on concentration field is revealed in Fig. 24. By enhancing β_c, concentration

boundary layer thickness and concentration distribution decline. The effect of chemical reaction τ for concentration profile is noted in Fig. 25. By increasing τ, the concentration field diminishes and it also declines in the thickness in concentration boundary zone.

Fig. 26 is prepared to examine the behavior of bio-convection Peclet number *Pe* on micro-organism distribution. A dwindle behavior is noted by variation of *Pe*. Physically Peclet number *Pe* and diffusivity of micro-organism has inverse relationship due to this micro-organism distribution decrease. To elaborate the impact of bio-convection Lewis number *Lb* on motile distribution, Fig. 27 is sketched. It is noted that for higher values of*Lb*causes lower micro-organism profile.

The numerical illustration of skin friction coefficient $-f''(0)$ for distinct values of *M*, λ, *Ha*, *A*, Λ, *Nr* and *Nc* are given in Table 1. It is observed that increasing values of *M*, *Ha*, *A* increase $-f''(0)$. Table 2 presents the numerical values of $-\theta'(0)$ for various values of *M*, λ, *Ha*, *A*, *Pr*, *Mb*, *Nt*, *Le* and β_t. A leading variation in $-\theta'(0)$ has been found out for *M*, *A*, *Pr* and β_t. From Table 3, where the variation in $-\phi'(0)$ has been observed. It is observed that $-\phi'(0)$ increases for *M*, *A*, *Nb* and *Le*. From Table 4, the numeric values of $-\chi'(0)$ are shown. It is clear from the table that for large values of *M* and *Lb*, $-\chi'(0)$ increases.

Table 5 Comparison of present values of skin friction coefficient for various values of λ and *M* when *Le* = 2.0, P_r = 1.7, *Nt* = *Nb* = 0.1 and *Ha* = β_t = β_c = *A* = Λ = δ = τ = 0

λ	*M*	Hayat *et al*. (2018)	Javed *et al*. (2013)	Ibrahim and Hindebu (2019)	Present results
0.0	0.2	−1.09545	−1.0954	−1.0955	−1.0955
0.1		−1.09395	−1.0940	−1.0940	−1.0940
0.2		−1.09245	−1.0924	−1.0925	−1.0925
0.3		−1.09092	−1.0909	−1.0909	−1.0909
0.4		−1.08938	−1.0894	−1.0894	−1.0894
0.5		−1.08782	−1.0878	−1.0878	−1.0878
0.6		−1.08625	−1.0862	−1.0863	−1.0863
0.7		−1.08465	−1.0847	−1.0847	−1.0847
0.0	0.4	−1.18322	−1.1832	−1.1833	−1.1833
0.1		−1.18034	−1.1808	−1.1809	−1.1809
0.2		−1.17843	−1.1784	−1.1785	−1.1785
0.3		−1.17598	−1.1776	−1.1760	−1.1760
0.4		−1.17349	−1.1735	−1.1735	−1.1735
0.5		−1.17096	−1.1710	−1.1710	−1.1710
0.6		−1.16838	−1.1684	−1.1684	−1.1684
0.7		−1.16575	−1.1658	−1.1658	−1.1658
0.0	0.6	−1.26491	−1.2649	−1.2650	−1.2649
0.1		−1.26199	−1.2620	−1.2621	−1.2620
0.2		−1.25902	−1.2590	−1.2591	−1.2590
0.3		−1.25600	−1.2560	−1.2561	−1.2560
0.4		−1.25291	−1.2529	−1.2530	−1.2529
0.5		−1.24976	−1.2498	−1.2498	−1.2498
0.6		−1.24655	−1.2466	−1.2466	−1.2466
0.7		−1.24327	−1.2433	−1.2434	−1.2433

5. Summary and conclusions

In this article, some remarkable features of motile microorganism of Eyring-Powell nanoliquid flow towards a stretchable cylinder with Cattaneo-Christov heat flux and heat absorption/generation impact has been investigated. The homotopy analysis approach is adopted to evaluate the solution of constituted flow problem. From the present analysis, the important results are listed below: The local Nusselt number increases for higher values of thermal relaxation parameter, curvature parameter, Prandtl number and Eyring-Powell nanoliquid parameter. The concentration distribution shown an increasing behavior as the thermophoresis parameter and magnetic parameter enhances while it depicts a dwindle trend for large values of Lewis number, Brownian motion, Eyring-Powell nanoliquid parameter and chemical reaction parameter. The skin friction coefficient increases for increment in magnetic parameter, mixed convection parameter and Eyring-Powell nanoliquid parameter while it shows a decreasing trend as the fluid parameter, buoyancy parameter, bio-convected Rayleigh number and curvature parameter enhance. The velocity distribution shows an increasing trend for higher values of a Powell-Eyrimg liquid parameter however, we observed its graph in decline manner when values of the fluid parameter, mixed convection parameter, buoyancy parameter, bio-convected Rayleigh number and magnetic parameter are increasing. The temperature field and thermal boundary layer thickness depict a decline trend with enlarge values of thermal relaxation parameter, Prandtl number, Powell-Eyring nanoliquid parameter and heat absorption parameter Temperature field and thermal boundary layer thickness shows an increasing trend for higher values of Brownian motion, thermophoresis parameter, magnetic parameter, curvature parameter and heat generation parameter. The Sherwood number indicates an increasing trend with an increasing value of curvature parameter, Lewis number, concentration relaxation parameter, Brownian motion parameter, and Eyring-Powell fluid parameter. For large values of bio-convected Lewis number, motile density number enhances.

Declaration of conflicting interests

The author(s) declared no potential conflicts of interest with respect to the research, authorship, and/or publication of this article.

Acknowledgments

This project was supported by the Deanship of Scientific Research at Prince Sattam Bin Abdulaziz University under the research project No 16794/01/2020.

References

Abbas, S.Z., Khan, M.I., Kadry, S., Khan, W.A., Israr-Ur-Rehman, M. and Waqas, M. (2020), “Fully developed entropy optimized

second order velocity slip MHD nanofluid flow with activation energy", *Comput. Methods Programs Biomed.*, **190**, 105362. https://doi.org/10.1016/j.cmpb.2020.105362.

Abdul Latiff, N.A., Uddin, M.J., Bég, O.A. and Ismail, A.I. (2016), "Unsteady forced bioconvection slip flow of a micropolar nanofluid from a stretching/shrinking sheet", *Proc. Inst. Mech. Eng. Part N J. Nanomater. Nanoeng. Nanosyst.*, **230**(4), 177-187. https://doi.org/10.1177/1740349915613817.

Ahmad Khan, J., Mustafa, M., Hayat, T. and Alsaedi, A. (2015), "Numerical study of Cattaneo-Christov heat flux model for viscoelastic flow due to an exponentially stretching surface", *PLOS One*, **10**(9), e0137363. https://doi.org/10.1371/journal.pone.0137363.

Ahmed, S.E. and Mahdy, A. (2016), "Laminar MHD natural convection of nanofluid containing gyrotactic microorganisms over vertical wavy surface saturated non-Darcian porous media", *Appl. Math. Mech.*, **37**(4), 471-484. https://doi.org/10.1007/s10483-016-2044-9.

Ahmed, Z., Nadeem, S., Saleem, S. and Ellahi, R. (2019), "Numerical study of unsteady flow and heat transfer CNT-based MHD nanofluid with variable viscosity over a permeable shrinking surface", *Int. J. Num. Methods Heat Fluidflow*, **29**(12), 4607-4623. https://doi.org/10.1108/HFF-04-2019-0346.

Akbar, N.S., Ebaid, A. and Khan, Z.H. (2015), "Numerical analysis of magnetic field effects on Eyring-Powell fluid flow towards a stretching sheet", *J. Magn. Magn. Mater.*, **382**, 355-358. https://doi.org/10.1016/j.jmmm.2015.01.088.

Al-Mdallal, Q., Aman, S., Al Fahel, S., Dadoa, S. and Kreishan, T. (2019), "Numerical study of unsteady flow of a fluid over shrinking long cylinder in a porous medium undermagnetic force", *J. Nanofluids*, **8**(7), 1609-1615. https://doi.org/10.1166/jon.2019.1712.

Alkanhal, T.A., Sheikholeslami, M., Usman, M., Haq, R.U., Shafee, A., Al-Ahmadi, A.S. and Tlili, I. (2019), "Thermal management of MHD nanofluid within the porous medium enclosed in a wavy shaped cavity with square obstacle in the presence of radiation heat source", *Int. J. Heat Mass Transf.*, **139**, 87-94. https://doi.org/10.1016/j.ijheatmasstransfer.2019.05.006.

Alwatban, A.M., Khan, S.U., Waqas, H. and Tlili, I. (2019), "Interaction of Wu's slip features in bioconvection of Eyring Powell nanoparticles with activation energy", *Processes*, **7**(11), 859. https://doi.org/10.3390/pr7110859.

Aziz, A., Alsaedi, A., Muhammad, T. and Hayat, T. (2018), "Numerical study for heat generation/absorption in flow of nanofluid by a rotating disk", *Results Phys.*, **8**, 785-792. https://doi.org/10.1016/j.rinp.2018.01.009.

Begum, N., Siddiqa, S. and Hossain, M.A. (2017), "Nanofluid bioconvection with variable thermophysical properties", *J. Mol. Liq.*, **231**, 325-332. https://doi.org/10.1016/j.molliq.2017.02.016.

Benmansour, D.L., Kaci, A., Bousahla, A.A., Heireche, H., Tounsi, A., Alwabli, A.S., Alhebshi, A.M., Al-ghmady, K. and Mahmoud, S.R. (2019), "The nano scale bending and dynamic properties of isolated protein microtubules based on modified strain gradient theory", *Adv. Nano Res., Int. J.*, **7**(6), 443-457. https://doi.org/10.12989/anr.2019.7.6.443.

Besthapu, P., Haq, R.U., Bandari, S. and Al-Mdallal, Q.M. (2019), "Thermal radiation and slip effects on MHD stagnation point flow of non-Newtonian nanofluid over a convective stretching surface", *Neural Comput. Appl.*, **31**(1), 207-217. https://doi.org/10.1016/j.physe.2014.07.013.

Cattaneo, C. (1948), "Sulla conduzione del calore", *Atti Sem. Mat. Fis. Univ. Modena*, **3**, 83-101.

Chaudhary, M.A. and Merkin, J.H. (1995), "A simple isothermal model for homogeneous-heterogeneous reactions in boundary-layer flow I Equal diffusivities", *Fluid Dyn. Res.*, **16**(6), 311. https://doi.org/10.1016/0169-5983(95)00015-6.

Choi, S.U. and Eastman, J.A. (1995), "Enhancing thermal conductivity of fluids with nanoparticles (No. ANL/MSD/CP-84938; CONF-951135-29)", Argonne National Lab., Illinois, USA.

Christov, C.I. (2009), "On frame indifferent formulation of the Maxwell-Cattaneo model of finite-speed heat conduction", *Mech. Res. Commun.*, **36**(4), 481-486. https://doi.org/10.1016/j.mechrescom.2008.11.003.

Doh, D.H., Muthtamilselvan, M., Swathene, B. and Ramya, E. (2020), "Homogeneous and heterogeneous reactions in a nanofluid flow due to a rotating disk of variable thickness using HAM", *Math. Comput. Simul.*, **168**, 90-110. https://doi.org/10.1016/j.matcom.2019.08.005.

Ebrahimi, F., Dabbagh, A., Rabczuk, T. and Tornabene, F. (2019), "Analysis of propagation characteristics of elastic waves in heterogeneous nanobeams employing a new two-step porosity-dependent homogenization scheme", *Adv. Nano Res., Int. J.*, **7**(2), 135-143. https://doi.org/10.12989/anr.2019.7.2.135.

Elnajjar, E.J., Al-Mdallal, Q.M. and Allan, F.M. (2016), "Unsteady flow and heat transfer characteristics of fluid flow over a shrinking permeable infinite long cylinder", *J. Heat Transf.*, **138**(9), 091008. https://doi.org/10.1115/1.4033058.

Eltaher, M.A., Almalki, T.A., Ahmed, K.I. and Almitani, K.H. (2019), "Characterization and behaviors of single walled carbon nanotube by equivalent-continuum mechanics approach", *Adv. Nano Res., Int. J.*, **7**(1), 39-49. https://doi.org/10.12989/anr.2019.7.1.039.

Freidoonimehr, N., Rashidi, M.M. and Mahmud, S. (2015), "Unsteady MHD free convective flow past a permeable stretching vertical surface in a nano-fluid", *Int. J. Therm. Sci.*, **87**, 136-145. https://doi.org/10.1016/j.ijthermalsci.2014.08.009.

Ghadikolaei, S.S., Yassari, M., Sadeghi, H., Hosseinzadeh, K. and Ganji, D.D. (2017), "Investigation on thermophysical properties of TiO_2-Cu/H_2O hybrid nanofluid transport dependent on shape factor in MHD stagnation point flow", *Powder Technol.*, **322**, 428-438. https://doi.org/10.1016/j.powtec.2017.09.006.

Han, S., Zheng, L., Li, C. and Zhang, X. (2014), "Coupled flow and heat transfer in viscoelastic fluid with Cattaneo-Christov heat flux model", *Appl. Math. Lett.*, **38**, 87-93. https://doi.org/10.1016/j.aml.2014.07.013.

Hayat, T., Anwar, M.S., Farooq, M. and Alsaedi, A. (2014), "MHD stagnation point flow of second grade fluid over a stretching cylinder with heat and mass transfer", *Int. J. Nonlinear Sci. Num. Simul.*, **15**(6), 365-376. https://doi.org/10.1515/ijnsns-2013-0104.

Hayat, T., Saeed, Y., Alsaedi, A. and Asad, S. (2015), "Effects of convective heat and mass transfer in flow of Powell-Eyring fluid past an exponentially stretching sheet", *PLoS One*, **10**(9), e0133831. https://doi.org/10.1371/journal.pone.0133831.

Hayat, T., Gull, N., Farooq, M. and Ahmad, B. (2016), "Thermal radiation effect in MHD flow of Powell-Eyring nanofluid induced by a stretching cylinder", *J. Aerosp. Eng.*, **29**(1), 04015011. https://doi.org/10.1061/(ASCE)AS.1943-5525.0000501.

Hsiao, K.L. (2014), "Nanofluid flow with multimedia physical features for conjugate mixed convection and radiation", *Comput. Fluids*, **104**, 1-8. https://doi.org/10.1016/j.compfluid.2014.08.001.

Hsiao, K.L. (2016), "Stagnation electrical MHD nanofluid mixed convection with slip boundary on a stretching sheet", *Appl. Therm. Eng.*, **98**, 850-861. https://doi.org/10.1016/j.applthermaleng.2015.12.138.

Hsiao, K.L. (2017), "Micropolar nanofluid flow with MHD and

viscous dissipation effects towards a stretching sheet with multimedia feature", *Int. J. Heat Mass Transf.*, **112**, 983-990. https://doi.org/10.1016/j.ijheatmasstransfer.2017.05.042.

Huaxu, L., Fuqiang, W., Dong, Z., Ziming, C., Chuanxin, Z., Bo, L. and Huijin, X. (2020), "Experimental investigation of cost-effective ZnO nanofluid based spectral splitting CPV/T system", *Energy*, **194**, 116913. https://doi.org/10.1016/j.energy.2020.116913.

Ibrahim, W. and Hindebu, B. (2019), "Magnetohydrodynamic (MHD) boundary layer flow of eyring-powell nanofluid past stretching cylinder with cattaneo-christov heat flux model", *Nonlin. Eng.*, **8**(1), 303-317. https://doi.org/10.1515/nleng-2017-0167.

Javed, T., Ali, N., Abbas, Z. and Sajid, M. (2013), "Flow of an Eyring-Powell non-Newtonian fluid over a stretching sheet", *Chem. Eng. Commun.*, **200**(3), 327-336. https://doi.org/10.1080/00986445.2012.703151.

Khan, W.A. and Pop, I. (2010), "Boundary-layer flow of a nanofluid past a stretching sheet", *Int. J. Heat Mass Transf.*, **53**(11-12), 2477-2483. https://doi.org/10.1016/j.ijheatmasstransfer.2010.01.032.

Khan, M.I., Kumar, A., Hayat, T., Waqas, M. and Singh, R. (2019), "Entropy generation in flow of Carreau nanofluid", *J. Mol. Liq.*, **278**, 677-687. https://doi.org/10.1016/j.molliq.2018.12.109.

Khan, N.S., Shah, Q., Bhaumik, A., Kumam, P., Thounthong, P. and Amiri, I. (2020), "Entropy generation in bioconvection nanofluid flow between two stretchable rotating disks", *Sci. Rep.*, **10**(1), 1-26. https://doi.org/10.1038/s41598-020-61172-2.

Kuznetsov, A.V. (2010), "The onset of nanofluid bioconvection in a suspension containing both nanoparticles and gyrotactic microorganisms", *Int. Commun. Heat Mass Transf.*, **37**(10), 421-1425. https://doi.org/10.1016/j.icheatmasstransfer.2010.08.015.

Kuznetsov, A.V. and Nield, D.A. (2010), "Natural convective boundary-layer flow of a nanofluid past a vertical plate", *Int. J. Therm. Sci.*, **49**(2), 243-247. https://doi.org/10.1016/j.ijthermalsci.2009.07.015.

Liao, S. (2014). *Advances in the Homotopy Analysis Method*, World Scientific, Singapore.

Ma, Y., Mohebbi, R., Rashidi, M.M., Yang, Z. and Sheremet, M.A. (2019), "Numerical study of MHD nanofluid natural convection in a baffled U-shaped enclosure", *Int. J. Heat Mass Transf.*, **130**, 123-134. https://doi.org/10.1016/j.ijheatmasstransfer.2018.10.072.

Malik, M.Y., Hussain, A. and Nadeem, S. (2013), "Boundary layer flow of an Eyring-Powell model fluid due to a stretching cylinder with variable viscosity", *Scientia Iranica*, **20**(2), 313-321. https://doi.org/10.1016/j.scient.2013.02.028.

Mishra, S.R., Khan, I., Al-Mdallal, Q.M. and Asifa, T. (2018), "Free convective micropolar fluid flow and heat transfer over a shrinking sheet with heat source", *Case Stud Therm Eng*, **11**, 113-119.

Mittal, A.S. (2019), "Analysis of water-based composite MHD fluid flow using HAM", *Int. J. Ambient Energy*, **2019**, 1-13. https://doi.org/10.1080/01430750.2019.1611648.

Mustafa, T. (2016), "Equivalences and correspondences between the deforming body induced flow and heat in two-three dimensions", *Phys. Fluids*, **28**(4), 043102. https://doi.org/10.1063/1.4945650.

Nadeem, S., Abbas, N. and Malik, M.Y. (2020), "Inspection of hybrid based nanofluid flow over a curved surface", *Comput. Methods Programs Biomed.*, **189**, 105193. https://doi.org/10.1016/j.cmpb.2019.105193.

Prasher, R., Song, D., Wang, J. and Phelan, P. (2006), "Measurements of nanofluid viscosity and its implications for thermal applications", *Appl. Phys. Lett.*, **89**(13), 133108. https://doi.org/10.1063/1.2356113.

Ragupathi, P., Hakeem, A.A., Al-Mdallal, Q.M., Ganga, B. and Saranya, S. (2019), "Non-uniform heat source/sink effects on the three-dimensional flow of Fe_3O_4/Al_2O_3 nanoparticles with different base fluids past a Riga plate", *Case Stud. Therm. Eng.*, **15**, 100521. https://doi.org/10.1016/j.csite.2019.100521,

Reddy, B.S.K., Krishna, M.V., Rao, K.S.N. and Vijaya, R.B. (2018), "RETRACTED: HAM Solutions on MHD flow of nano-fluid through saturated porous medium with hall effects", *Mater. Today*, 5(1), 120-131. https://doi.org/10.1016/j.matpr.2017.11.062.

Rehman, K.U., Al-Mdallal, Q.M. and Malik, M.Y. (2019), "Symmetry analysis on thermally magnetized fluid flow regime with heat source/sink", *Case Stud. Therm. Eng.*, **14**, 100452. https://doi.org/10.1016/j.csite.2019.100452.

Riaz, A., Ellahi, R., Bhatti, M.M. and Marin, M. (2019), "Study of heat and mass transfer in the Eyring-Powell model of fluid propagating peristaltically through a rectangular compliant channel", *Heat Transf. Res.*, **50**(16), 1539-1560. https://doi.org/10.1615/HeatTransRes.2019025622.

Safaei, B., Khoda, F.H. and Fattahi, A.M. (2019), "Non-classical plate model for single-layered graphene sheet for axial buckling". *Adv. Nano Res., Int. J.*, **7**(4), 265-275. https://doi.org/10.12989/anr.2019.7.4.265.

Saranya, S. and Al-Mdallal, Q.M. (2020), "Non-Newtonian ferrofluid flow over an unsteady contracting cylinder under the influence of aligned magnetic field", *Case Stud. Therm. Eng.*, **21**, 100679. https://doi.org/10.1016/j.csite.2020.100679.

Shah, Z., Dawar, A., Kumam, P., Khan, W. and Islam, S. (2019), "Impact of nonlinear thermal radiation on MHD nanofluid thin film flow over a horizontally rotating disk", *Appl. Sci.*, **9**(8), 1533. https://doi.org/10.3390/app9081533.

Shahsavari, D., Karami, B. and Janghorban, M. (2019), "Size-dependent vibration analysis of laminated composite plates", *Adv. Nano Res., Int. J.*, **7**(5), 337-349. https://doi.org/10.12989/anr.2019.7.5.337.

Shehzad, S.A. (2018), "Magnetohydrodynamic Jeffrey nanoliquid flow with thermally radiative Newtonian heat and mass species", *Revista Mexicana Física*, **64**(6), 628-633. http://dx.doi.org/10.31349/revmexfis.64.628.

Soomro, F.A., Haq, R.U., Al-Mdallal, Q.M. and Zhang, Q. (2018), "Heat generation/absorption and nonlinear radiation effects on stagnation point flow of nanofluid along a moving surface", *Results Phys.*, **8**, 404-414. https://doi.org/10.1016/j.rinp.2017.12.037.

Straughan, B. (2008), *Stability and Wave Motion in Porous Media*, Springer Science & Business Media, Durham, UK.

Straughan, B. (2010), "Thermal convection with the Cattaneo-Christov model", *Int. J. Heat Mass Transf.*, **53**(1-3), 95-98. https://doi.org/10.1016/j.ijheatmasstransfer.2009.10.001.

Subhani, M. and Nadeem, S. (2019), "Numerical analysis of micropolar hybrid nanofluid", *Appl. Nanosci.*, **9**(4), 447-459. https://doi.org/10.1007/s13204-018-0926-2.

Tlili, I., Ramzan, M., Kadry, S., Kim, H.W. and Nam, Y. (2020), "Radiative MHD nanofluid flow over a moving thin needle with Entropy generation in a porous medium with dust particles and Hall current", *Entropy*, **22**(3), 354. https://doi.org/10.3390/e22030354.

Turkyilmazoglu, M. (2016a), "Determination of the correct range of physical parameters in the approximate analytical solutions of nonlinear equations using the Adomian decomposition method", *Mediterranean J. Math.*, **13**(6), 4019-4037. https://doi.org/10.1007/s00009-016-0730-8.

Turkyilmazoglu, M. (2016b), "Equivalences and correspondences between the deforming body induced flow and heat in two-three dimensions", *Phys. Fluids*, **28**(4), 043102. https://doi.org/10.1063/1.4945650.

Umar, M., Akhtar, R., Sabir, Z., Wahab, H.A., Zhiyu, Z., Imran, A., Shoaib, M. and Raja, M.A.Z. (2019), "Numerical treatment

for the three-dimensional Eyring-Powell fluid flow over a stretching sheet with velocity slip and activation energy", *Adv. Math. Phys*., 2019, 9860471. https://doi.org/10.1155/2019/9860471.

Zangooee, M.R., Hosseinzadeh, K. and Ganji, D.D. (2019), "Hydrothermal analysis of MHD nanofluid (TiO_2-GO) flow between two radiative stretchable rotating disks using AGM", *Case Stud. Therm. Eng.*, **14**, 100460. https://doi.org/10.1016/j.csite.2019.100460.

Zhao, G., Wang, Z. and Jian, Y. (2019), "Heat transfer of the MHD nanofluid in porous microtubes under the electrokinetic effects", *Int. J. Heat Mass Transf.*, **130**, 821-830. https://doi.org/10.1016/j.ijheatmasstransfer.2018.11.007.

Zubair, M., Ijaz, M., Abbas, T. and Riaz, A. (2019), "Analysis of modified Fourier law in flow of ferromagnetic Powell-Eyring fluid considering two equal magnetic dipoles", *Can. J. Phys*., **97**(7), 772-776. https://doi.org/10.1139/cjp-2018-0586.

CC